REPORT DOCUMENTATION PAGE

AFRL-SR-AR-TR-05-

0196

Public reporting burden for this collection of information is estimated to average 1 hour per response, including th gathering and maintaining the data needed, and completing and reviewing the collection of information. Send cor collection of information, including suggestions for reducing this burden, to Washington Headquarters Services, Di Davis Highway, Suite 1204, Arlington, VA 22202-4302, and to the Office of Management and Budget, Paperwork

1. AGENCY USE ONLY *(Leave blank)*	2. REPORT DATE	3. REPORT TYPE AND DATES COVERED
		15 SEP 2001 - 14 SEP 2004 FINAL

4. TITLE AND SUBTITLE
(Bio-Inspired Theme) Studies of Biological reponse to External Electronic Fields for Cellular Manipulation and Diagnostics based on a Multidimensional Electromagnetic Model

5. FUNDING NUMBERS
61102F
2312/TX

6. AUTHOR(S)
DR JOSHI

7. PERFORMING ORGANIZATION NAME(S) AND ADDRESS(ES)
OLD DOMINION UNIVERSITY
RESEARCH FOUNDATION
800 WEST 46TH ST PO BOX 6369
NORFOLK VA 23508-0369

8. PERFORMING ORGANIZATION REPORT NUMBER

9. SPONSORING/MONITORING AGENCY NAME(S) AND ADDRESS(ES)
AFOSR/NE
4015 WILSON BLVD
SUITE 713
ARLINGTON VA 22203

10. SPONSORING/MONITORING AGENCY REPORT NUMBER
F49620-01-1-0506

11. SUPPLEMENTARY NOTES

12a. DISTRIBUTION AVAILABILITY STATEMENT
DISTRIBUTION STATEMENT A: Unlimited

12b. DISTRIBUTION CODE

13. ABSTRACT *(Maximum 200 words)*

A comprehensive modeling and experimental effort was carried out to develop an understanding of cellular bio-response to short duration, high-intensity electric fields. Macroscopic models for determining the time-dependent spatially-variable electric potential and current flows at single cells were developed. This provides predictions of both transmembrane voltages and temperature changes. The macroscopic model was coupled to a nano-simulator to probe the sub-cellular response at the molecular level. Many of the observed details such as PS externalization, the time scales for pore formation, and their probable diameters were predicted. The relevant parameters of the bio-system were obtained within our group by developing the Time Domain Dielectric Spectroscopy method. The system is operational, and yields data on the conductivity and permittivities of cells and its organelles. This is a useful and important development. Cellular response were measured based on a variety of techniques, including flow cytometry, optical microscopy and imaging. The central results were: (i) There is a critical electric field and pulse duration for cell death. (ii) The critical voltage reduces for multiple pulses and increasing pulse width. (iii) PS externalization leading to cell death can be electrically triggered. (iv) Pore formation can be reversible for short nano-second pulses.

This study would be indicative of the following conclusions: (i) It may be energy efficient to use short pulses for cell death. (ii) Selective apoptotic targeting of cells appears to be possible. (iii) Non-uniform internal potentials (arising from dipole and charge placements) promote cellular transport. Hence, their modification/disruption through molecular conformational change would alter cell functioning.

14. SUBJECT TERMS

15. NUMBER OF PAGES

16. PRICE CODE

17. SECURITY CLASSIFICATION OF REPORT	18. SECURITY CLASSIFICATION OF THIS PAGE	19. SECURITY CLASSIFICATION OF ABSTRACT	20. LIMITATION OF ABSTRACT
Unclassified	Unclassified	Unclassified	UL

Old Dominion University

Department of Electrical & Computer Engineering

AFOSR Bio-Inspired Concepts: Studies of Biological Response to External Electric Fields for Cellular Manipulation and Diagnostics – Modeling and Experimentation

Final Technical Report*
1 September 2001 – 15 February 2005

3 May, 2005

Submitted by:
Ravindra Joshi — Principal Investigator and Professor
Department of Electrical and Computer Engineering
Old Dominion University
Norfolk, VA 23529
Tel. (757) 683-4827
Fax: (757) 683-3220
E-mail: rjoshi@odu.edu

DISTRIBUTION STATEMENT A
Approved for Public Release
Distribution Unlimited

*The views and conclusions contained in this report are those of the authors and should not be interpreted as necessarily representing the official policies or endorsements, either expressed or implied, of the Air Force Research Laboratory or the U.S. Government.

TABLE OF CONTENTS

INTRODUCTION.....4

LIST OF OBJECTIVES AND ACCOMPLISHMENTS.....4
Objective I: Modeling for Cellular Response to External Electric Fields.....4
Accomplishments Under Objective I. 4
A. Development of a Macroscopic, Distributed Cell Model.....4
B. Energy Landscape Calculations for Pulse-Width Dependence.....10
C. Implementation of Molecular Dynamics Simulations for Membrane Response 14
Objective II: Time Domain Dielectric Spectroscopy.....20
Accomplishments Under Objective II.....20
Objective III: Cellular Measurements of High-Field Pulse Effects.....22
Accomplishments Under Objective III.....22

SUMMARY ... .26

REFERENCES.....27

PERSONNEL.....30
PUBLICATIONS.....30
INTERACTIONS RELATED TO PROJECT.....33
RECOGNITION.....34
NEW DISCOVERIES, INVENTIONS AND PATENTS.....34

INTRODUCTION

This final technical report describes work carried out on the Bio-Inspired Concepts grant titled "Studies of Biological Response to External Electric Fields for Cellular Manipulation and Diagnostics – Modeling and Experimentation." Significant progress (both in experimental activities and in theoretical modeling) has been made at Old Dominion University, in conjunction with Eastern Virginia Medical School, and is described in detail in this report.

LIST OF OBJECTIVES AND ACCOMPLISHMENTS

Objective 1: Modeling for Cellular Response to External Electric Fields

Appropriate bio-models for the analysis of cellular response to high-intensity, short-duration, external electric fields were developed. The focus was on the three distinct tasks: (a) Development of numerical codes for three-dimensional, time-dependent solution of distributed potentials and current flows in a cell. These models can also be applied to the evaluation of current-voltage characteristics of membrane pores. Polarity dependencies and asymmetric behavior resulting for internal fixed-charge distributions and non-uniformities in pore cross-sectional area can be probed. (b) Use of the distributed electrical model as the input to predict cell irreversibility and its pulse-width dependence based on a simple two-valley energy model, and (c) Development of Molecular Dynamics simulation codes for microscopic analysis at the atomic level of cell membranes. The dynamics of pore formation, the anode-side preference, and mechanism of phosphotidylserine (PS) externalization was examined

Accomplishments Under Objective 1

(A) Development of a Macroscopic, Distributed Cell Model:

All of the three above tasks were successfully carried out. Models were developed and corresponding numerical codes implemented. The results and predictions obtained were published in various scientific journals [1-6]. Figure 1 shows a schematic for the distributed, three-dimensional, time-dependent model developed for analysis of voltages (including trans-membrane potentials) and current flows. A spherical simulation volume used for the calculations is shown with an axial electric field pulse encompassing a cell and an internal organelle. Pores have been shown in this schematic as a qualitative guide. The distributed electrical representation of the cell shown in Fig. 1, comprised of parallel resistive (R) and capacitive (C) elements. Based on the electric field and current distributions, the power dissipation could be calculated. The maximum temperature rise within the cell volume could also be computed. A typical result for a 225 kV/cm voltage pulse having a 1.5 ns rise time, a 10 ns ON time, and a 1.5 ns fall time is shown on Fig. 2 for a normal B-cell. The parameters for the B-cell were taken from the literature [7]. A maximum temperature rise of about 1.2 °K is predicted. The highest temperature rise is

predicted to occur just outside the cell, with the cytoplasm being a somewhat lower temperature, and the inner organelle having the least heating. In actual experiments, the

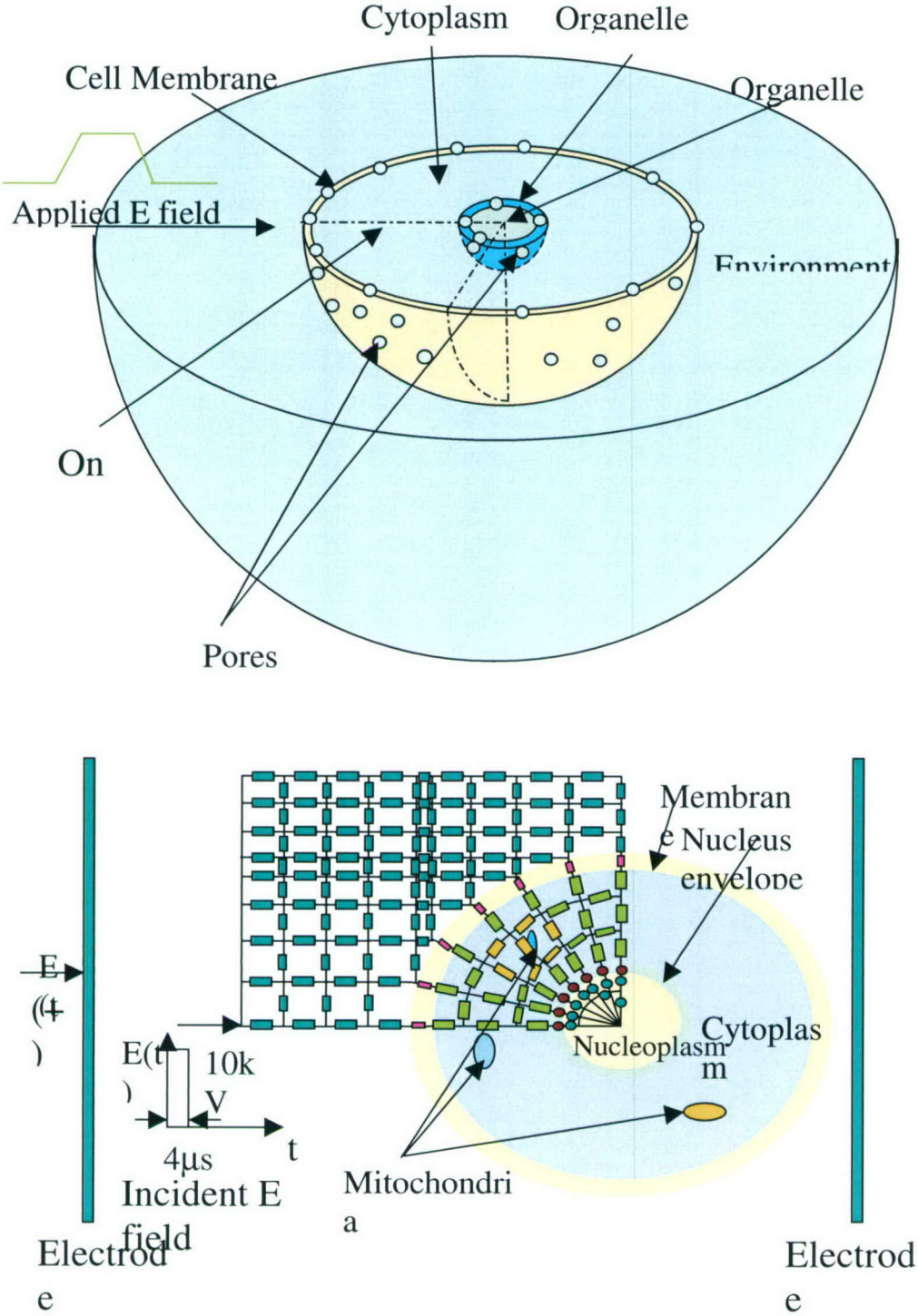

Fig. 1. Schematic for the cellular calculations. (a) The simulated region including the cell and an organelle, and (b) the distributed electrical representation.

voltages (V) are typically on the order of 100 kV/cm. Since the power dissipation scales as V^2, one can expect a maximum heating of about 0.3 °K. This is in line with the notion of an essentially non-thermal biological effect. Unfortunately, it is very difficult to obtain temperature measurements with temporal resolution on the nano-second time scales. Hence, experimental corroboration has not been possible so far.

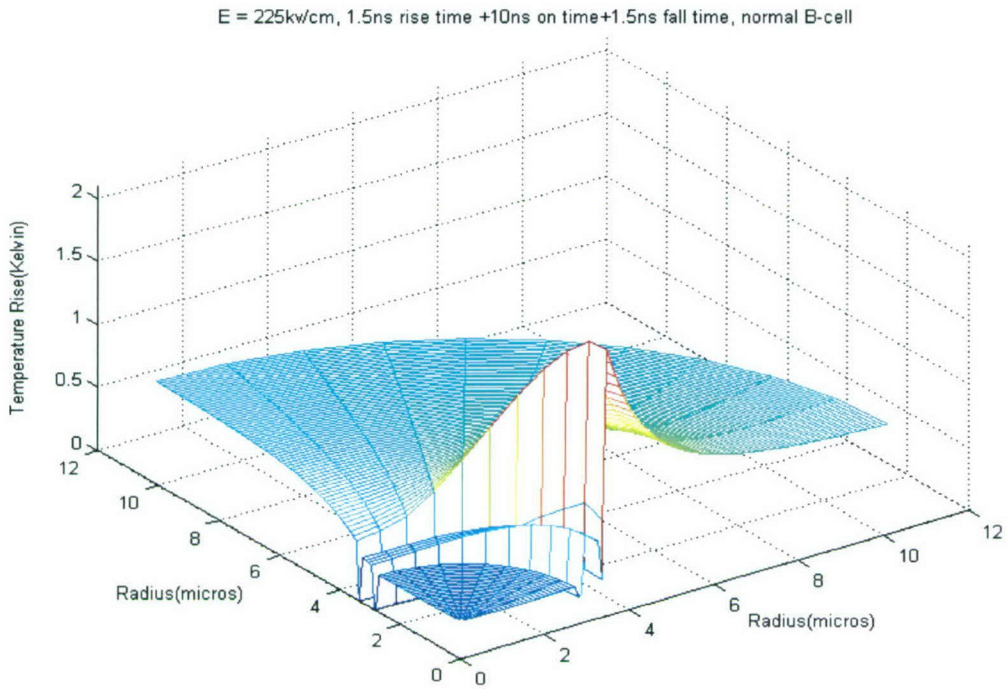

Fig. 2. Results of the temperature rise in response to an external voltage pulse.

The distributed, macroscopic electrical model of the cell was used to then used to simulate poration at both the outer (plasma) and the organelle membranes. A continuum approach based on the Smoluchowski equation [1,8-12] was used to model the pore dynamics. For purposes of numerical computations the entire cell was broken up into segments, and each segment represented by a parallel RC combination. Azimuthal symmetry was used to map the three-dimensional structure into the r and φ co-ordinates of a spherical system. This method is different from the Legendre polynomial model used in the past for electrostatic cases. Volume and shape changes of cells were ignored since the external applied pulse is too short (~ns) for cells to deform much during this time interval.

Time Dependent Electrical Calculations:

In our simulations, the computational region is a sphere that includes the cell, its sub-structure, and the surrounding suspension medium. It is discretized in r and θ direction as shown in Fig. 3. For simplicity, only a quarter of the computational region is

considered. For simplicity, membranes are taken as an integral unit, i.e., this sub-region is not further discretized. For each element, the current continuity equation given below holds:

$$\nabla \bullet (J + \frac{\partial D}{\partial t}) = 0 \quad , \tag{1}$$

where J is the current density and D the electric displacement vector. For nodes with index 0<i<n and 0<j<m, as shown in Fig. 3, the above equation can be rewritten in the following form :

$$\sum_{k=1}^{6} (\sigma E + \varepsilon \frac{\partial E}{\partial t})_k \times A_k = \sum_{k=1}^{6} I_k = 0 \quad . \tag{2}$$

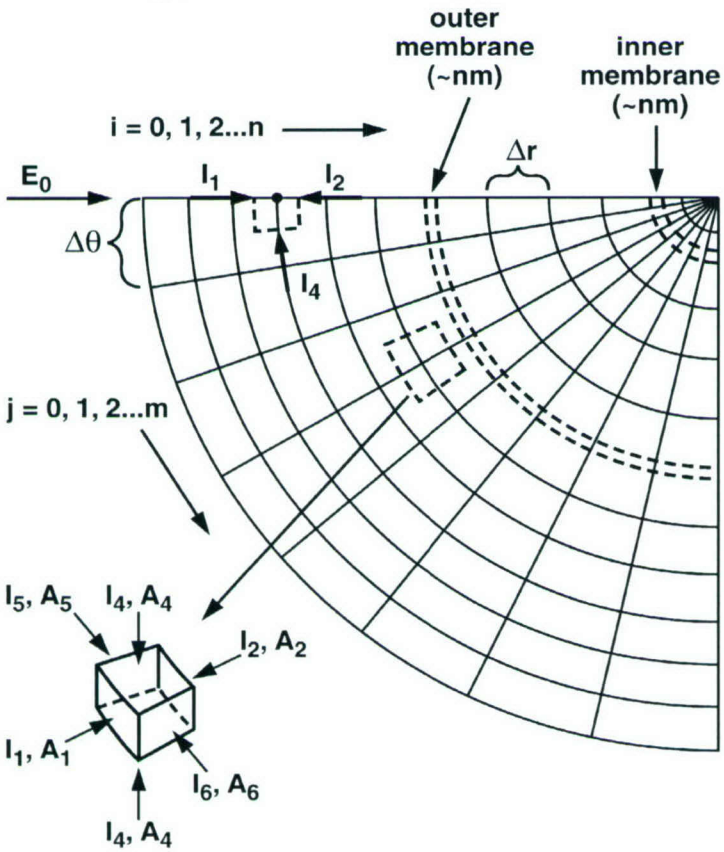

Figure 3: Schematic of one quarter of the model used to represent a cell for the distributed electrical calculations. The dotted box shows a typical element with current flows.

Here I_5 and I_6 are currents along the ϕ direction. Considerations of geometric symmetry of the computation region leads to $I_5 = I_6 = 0$ due to the equi-potentials. Consequently, one obtains the following equation discretized in space and time:

$$\sigma_1 \frac{V_{i-1,j}^t - V_{i,j}^t}{\Delta r} A_1 + \sigma_2 \frac{V_{i+1,j}^t - V_{i,j}^t}{\Delta r} A_2 + \sigma_3 \frac{V_{i,j-1}^t - V_{i,j}^t}{r\Delta\theta} A_3 + \sigma_4 \frac{V_{i,j+1}^t - V_{i,j}^t}{r\Delta\theta} A_4 +$$
$$\frac{\varepsilon_1}{\Delta t}[\frac{V_{i-1,j}^{t+1} - V_{i,j}^{t+1}}{\Delta r} - \frac{V_{i-1,j}^t - V_{i,j}^t}{\Delta r}]A_1 + \frac{\varepsilon_2}{\Delta t}[\frac{V_{i+1,j}^{t+1} - V_{i,j}^{t+1}}{\Delta r} - \frac{V_{i+1,j}^t - V_{i,j}^t}{\Delta r}]A_2 + \quad . \quad (3)$$
$$\frac{\varepsilon_3}{\Delta t}[\frac{V_{i,j-1}^{t+1} - V_{i,j}^{t+1}}{r\Delta\theta} - \frac{V_{i,j-1}^t - V_{i,j}^t}{r\Delta\theta}]A_3 + \frac{\varepsilon_4}{\Delta t}[\frac{V_{i,j+1}^{t+1} - V_{i,j}^{t+1}}{r\Delta\theta} - \frac{V_{i,j+1}^t - V_{i,j}^t}{r\Delta\theta}]A_4 = 0$$

In the above, $V_{i,j}^t$ stands for the potential at node (i, j) at time *t*. The radial distance between nodes (i, j) and (n, m) is *r*. The areas A_1 through A_4 are shown in Fig. 3. Also, σ_1 through σ_4, and ε_1 through ε_4 are the conductivities and permittivities, respectively, at faces 1-4. Thus, if a node were to be within the environment medium, then all the σ values would be the same. However, for nodes on a membrane, σ_1 would be different from σ_2.

In order to reduce the computation load, special boundary conditions were applied, and only a quarter of the entire spherical computational region was considered based on the inherent symmetry. Nodes with $j = 0$ and $j = m$ had to be treated carefully. Only I_1, I_2 and I_4 are nonzero since, the targeted element only has 5 faces as face 3 shrinks to a line. For $j = 0$ and $0 < i < n$, eqn. (3) becomes:

$$\sigma_1 \frac{V_{i-1,j}^t - V_{i,j}^t}{\Delta r}(r + \Delta r/2)^2(\cos\theta - \cos(\theta + \Delta\theta/2)) +$$
$$\sigma_2 \frac{V_{i+1,j}^t - V_{i,j}^t}{\Delta r}(r - \Delta r/2)^2(\cos\theta - \cos(\theta + \Delta\theta/2)) +$$
$$\sigma_4 \frac{V_{i,j+1}^t - V_{i,j}^t}{r\Delta\theta} r\Delta r \sin(\theta + d\theta/2) +$$
$$\frac{\varepsilon_1}{\Delta t}[\frac{V_{i-1,j}^{t+1} - V_{i,j}^{t+1}}{\Delta r} - \frac{V_{i-1,j}^t - V_{i,j}^t}{\Delta r}](r + \Delta r/2)^2(-1 - \cos(\theta + \Delta\theta/2)) + \quad (4)$$
$$\frac{\varepsilon_2}{\Delta t}[\frac{V_{i+1,j}^{t+1} - V_{i,j}^{t+1}}{\Delta r} - \frac{V_{i+1,j}^t - V_{i,j}^t}{\Delta r}](r - \Delta r/2)^2(-1 - \cos(\theta + \Delta\theta/2)) +$$
$$\frac{\varepsilon_4}{\Delta t}[\frac{V_{i,j+1}^{t+1} - V_{i,j}^{t+1}}{r\Delta\theta} - \frac{V_{i,j+1}^t - V_{i,j}^t}{r\Delta\theta}] r\Delta r \sin(\theta + \Delta\theta/2) = 0$$

In the above, $\theta = \pi + j \times \Delta\theta = \pi$ and $\Delta\theta$ is $\frac{\pi}{2}/m$. For an electric field applied applied along the z direction (as shown in Fig.3) and potential at node with $i = n$ is zero, i.e, $V_{n,j} = 0$. Nodes with index $j = 0$ are equi-potentials, so $V_{i,m} = V_{n,j} = 0$. Another boundary condition to be considered is for nodes with $i = 0$. The potentials of such nodes is calculated as: $V_{0,j} = -E_0 R\cos\theta$, for j = 0...m, where E_0 is the externally applied electrical field, and *R* the radius of the computational region.

Combining with the boundary conditions discussed above, one gets N equations for the N unknown node voltages. These N equations can easily be solved through matrix inversion of the form: Ax = B. Here A is a sparse coefficient matrix. Potential on each node is easily updated at each time step.

A summary of the results obtained for poration in normal and cancer cells due to different pulses at both the inner and outer membranes are given in Table I. Basically, the following trends are evident:

(i) It appears on the basis of the present results that the inner membrane of a normal, healthy cell is difficult to porate.

(ii) With increasing electric field, the inner organelle membrane can be porated. This should lead to possible apoptosis or cell death due to such ultra-short, high-intensity pulses.

(iii) Longer duration pulses are more likely to do more damage. For example, at the 100 kV/cm field, the 50 ns pulse is predicted to porate both the inner and outer membranes of the cancer B-cell, while a 10 ns duration would leave the inner membrane intact.

Table I

Normal B-cell	**Outer membrane**	**Inner Membrane**
E: 15kv/cm,	No	No
E: 45kv/cm,	Yes	No
E: 100kv/cm,	Yes	No
Cancer B-cell		
E: 45kv/cm,	Yes	No
E: 100kv/cm,	Yes	No
E: 45kv/cm,	Yes	No
E: 100kv/cm,	Yes	Yes
E: 225kv/cm, 1.5ns+10ns+1.5ns	Yes	Yes

The Dynamic Pore Model:

Coupling the above electrical model with the Smoluchowski equation (SE) for the growth and decay of pores leads to a dynamic simulation of the cell to an electrical pulse. The concept of using a diffusive motion across an energy landscape was originally proposed by Smoluchowski [8], reviewed by Chandrasekhar [9], and subsequently used by Kramers to develop the theory of activated transition rates in the limit of large friction. As a consequence of the fluctuating-dissipative nature of the bio-system, the evolution of the mechanical variables (the pore density in this case) can be expected to follow a diffusive Brownian motion across the energy landscape. The continuum Smoluchowski theory yields the following for the pore density distribution function n(r, t), with r being the pore radius [11,12]:

$$\frac{\partial n(r,t)}{\partial t} - \frac{D}{k_B T}\frac{\partial(n(r,t)\partial E(r)/\partial r)}{\partial r} - D\frac{\partial^2 n(r,t)}{\partial r^2} = S(r) \quad , \qquad (5)$$

where *S(r)* is the source (or pore formation) term, while *D* is a pore diffusion constant, and E(r) is the pore-formation energy. Details of the SE, its application and the dynamical aspects of electroporation have been addressed in a series of recent papers [1,5,6] by our group, and will not be reviewed here. The pore area A_p is governed by the pore density distribution function n(r,t), which in turn, obeys the Smoluchowski equation. It turns out that the dynamic pore area A_p is given by:

$$A_P(r,t) \sim A_0[\int_0^{r} 2\pi r^* n(r^*,t)dr^*] \quad , \qquad (6)$$

where A_0 is the equilibrium area under zero bias. As pores form in response to an externally applied electric pulse, the value of A_P increases, and the electrical conductivity through the pore becomes time-varying. The effective membrane conductivity $\sigma_{eff_mem}(t)$ can be calculated by:

$$\sigma_{eff_mem}(t) = \frac{A_P(r,t)}{A_0}\sigma_{out} + (1 - \frac{A_P(r,t)}{A_0})\sigma_{mem} \quad , \qquad (7)$$

where σ_{out} is the conductivity of the medium outside the membrane and σ_{mem} is the conductivity of the unporated membrane. Thus, the SE yields both the pore distribution and dynamic pore area, which in turn affects the electrical parameters. This is coupled to the distributed electrical analysis for self-consistency through dynamic variations of the resistance R and capacitance C.

(B) Energy Landscape Calculations for Pulse-Width Dependence:

The above macroscopic, distributed electrical model was applied to probe and analyze the pulse-width dependence of cellular response. Experimental data indicates

that for a given fixed pulse energy, cell apoptosis is more pronounced for longer pulses [13]. Some of the experimental results are shown in Fig. 4. The data shows caspase activity (an apoptosis marker) in Jurkat cells subjected to a single pulse of variable duration, but fixed total energy of 1.7 J/cc. Longer duration pulses are again seen to produce stronger apoptotic responses.

We have attempted to provide a simple, but physical model for cell irreversibility and apoptosis in response to an ultrashort (nanosecond), high-intensity electric pulse. We hypothesize that apoptotic behavior may be the result of irreversible conformational

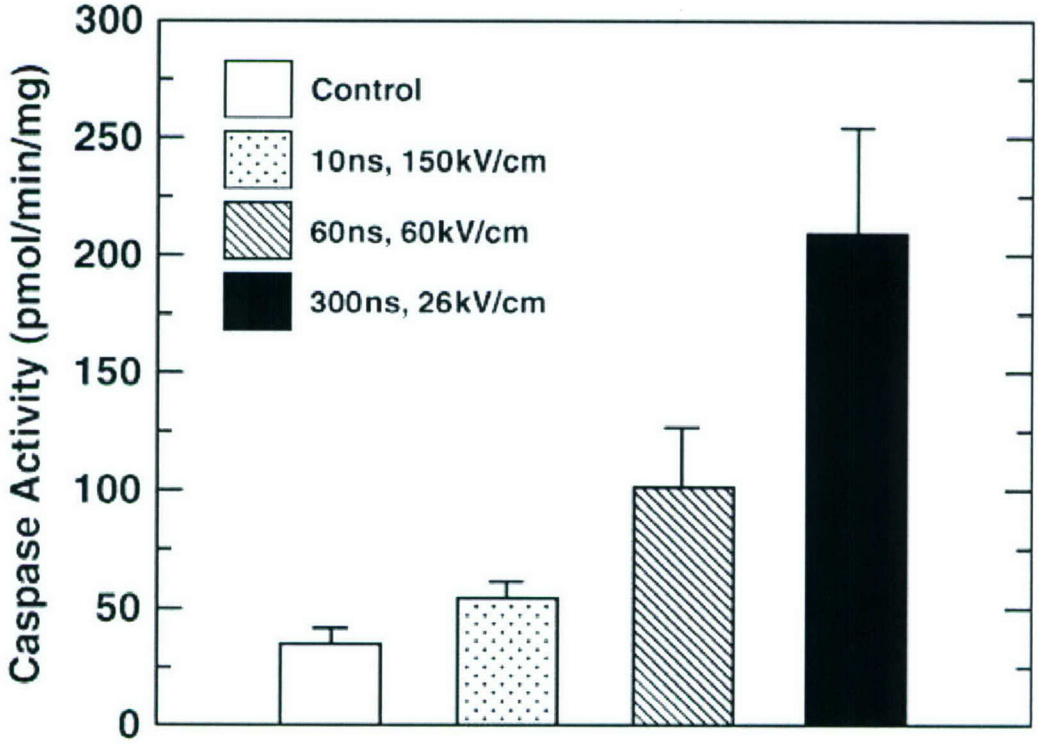

Fig. 4. Data showing caspase activity in Jurkat cells subjected to a single pulse of variable duration, but fixed total energy of 1.7 J/cc. Longer duration pulses are again seen to produce stronger apoptotic response.

changes at the inner mitochondrial membrane. Such changes are likely to be driven by the high electric fields that arise from strong transient increases in transmembrane potentials. Our approach was based on an energy landscape model, which is used to determine the temporal evolution of the configurational probability distribution function [5]. Such an energy landscape picture has been used in the description of protein changes [14], as well as the folding/unfolding of small globular proteins [15]. A comprehensive and accurate treatment of this problem is extremely difficult and challenging given that apoptosis can have several pathways, the sequential details of the bio-physics are not well known, and neither are the magnitudes of the internal energies and configurations. Given

the various difficulties, the present model merely attempted to provide a possible physical picture dependent only on the electrical trigger, and captured the experimentally observed pulse-width dependence.

Our model was probabilistic through the use of the Smoluchowski equation and, it coupled the distributed electrical model for current flow to provide the time-dependent trans-membrane voltages. The results are shown in Fig. 5, and agree with the observed experimental data very well. The probability for occupancy of a secondary energy minima within a complex energy landscape is shown. The initial state of the system has complete and total occupancy of the lowest energy valley. With energy supplied from the external electric-pulse, the occupancy shifts to higher energy, and some states in the secondary valley can be occupied. The barrier between the two adjacent valleys precludes complete recovery, and hence, an inherent irreversibility within the system results.

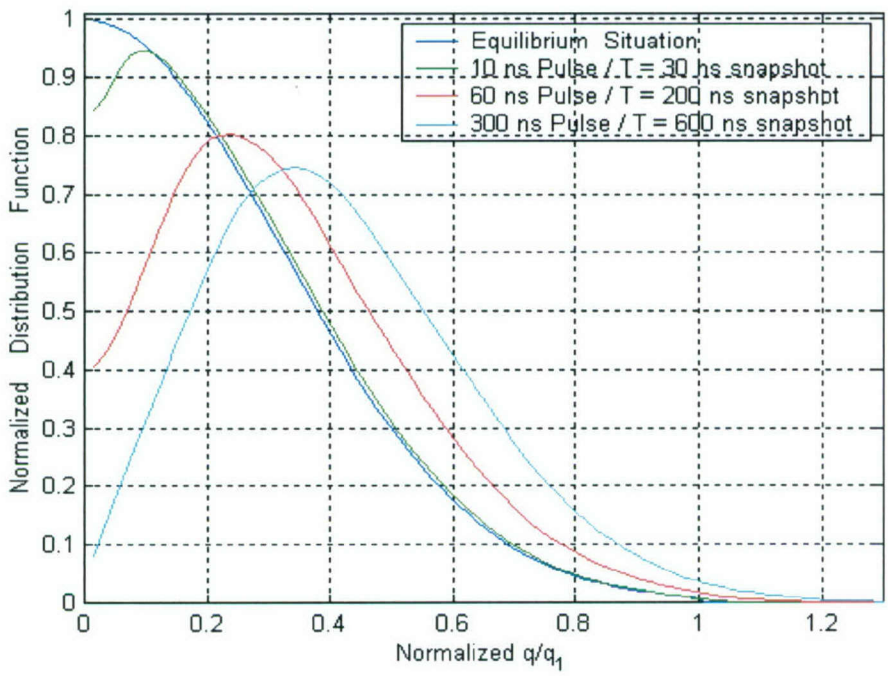

Figure 5a. Simulation results of the occupancy distribution within a two-valley, energy landscape model. (i) Snapshots of the equilibrium function and at various times following 10 ns, 60 ns and 300 ns pulses.

Based on the model developed, we predict a number of interesting features.

(i) First, cell irreversibility at a fixed input energy will depend on the pulse width, and is likely to have an optimal range. Pulses that are very short would not have a significant effect due to insufficient durations for electric field driven conformational changes. On the other hand, much slower and longer pulses would also be rendered ineffective due to their inability to penetrate the

membranes of the inner organnelles and develop a significant transmembrane voltage.

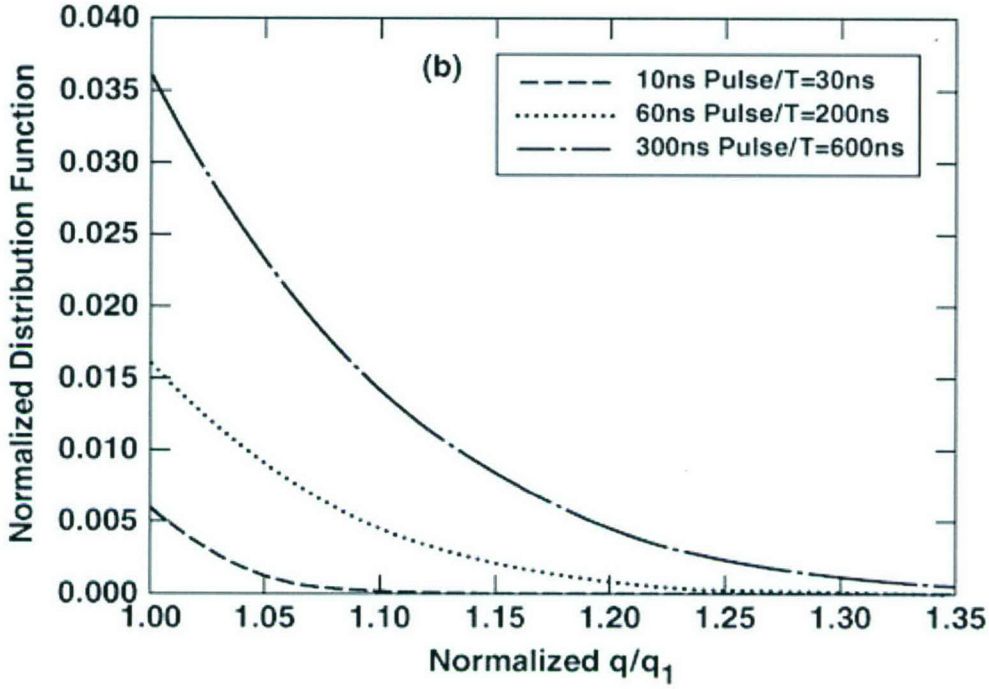

Figure 5b. Simulation results of the occupancy distribution within a two-valley, energy landscape model. Plots emphasizing higher configuration p(q) values within the secondary valley.

(ii) The electrical effects are likely to be cumulative and to exhibit a memory effect, provided successive pulses were to be applied with delay times less than that required for complete recovery of the p(q) profiles. Such a memory effect has indeed been noted in the context of the ultrashort, high-intensity pulsing.

(iii) The inherent probabilistic basis of this model implies that complete and total killing of cell populations can never be achieved by a single shot exposure. There will always be a finite probability distribution below the threshold because of the diffusive motion in energy space. Only at very low temperatures might one expect cohesive and "ballistic" motion. This prediction of incomplete killing is in keeping with experimental observations.

(iv) Furthermore, this model predicts that the use of very high electric field intensities may not necessarily have a significantly larger impact. This naturally follows since not only is the pulse duration an important factor, but also because the transmembrane potential would not scale with the applied field. Electroporation

and dynamic changes in conductivity would work to offset the impact of larger external fields.

(v) Here the irreversibility mechanism is taken to arise from fixed charge and dipole movements brought about within the membrane by the electrostatic driving force produced by the large transient transmembrane potentials. Consequently, excitation processes that cannot generate large electric fields at membranes, or if their time durations are small, might not be very effective in electrically triggering apoptotic behavior in cells. For example, under "contactless" conditions, or for microwave and radio-frequency excitation, cellular apoptosis may be expected to be fairly negligible.

(C) Implementation of Molecular Dynamics Simulations for Membrane Response:

Microscopic analysis based on the Molecular Dynamics atomistic approach was developed and applied to probe the membrane response. The microscopic MD simulation approach is superior to continuum approaches. Advantages of this approach are: (i) Inclusion of the collective, many-body interaction potentials at the nano-scale level, (ii) Dynamical screening, (iii) Avoidance of the "mean-field" approximations, (iv) A natural inclusion of noise and statistical fluctuations, (v) Self-consistent and dynamical transport calculations without arbitrary fitting parameters, and (vi) Easy incorporation of arbitrary defects and non-uniformities, as well as complex geometries.

In our studies, the GROMACS package [16,17] was used for the MD simulations of field-induced membrane effects. It was applied to dipalmitoyl-phosphatidyl-choline (DPPC) bilayers. Details of the dode-cylpho-sphocholine (DPC) force field for membrane molecular motion can be found elsewhere [18]. The system was coupled to an isotropic pressure bath of 1 atmosphere, and a heat bath of 300 K [19]. Velocities of the water and membrane molecules were scaled with a coupling constant of 0.1 ps. The algorithms for pressure and temperature control were those discussed by Allen and Tildesly [20]. A 2 fs time step was used with constrains on the bond lengths within the lipids and on the water geometry. A group based twin cutoff scheme was employed for the non-bonded interactions, with R_{cutoff} of 1.0 nm for Lennard-Jones, and R_{cutoff} of 1.5 nm for electrostatic interactions. The SPC water model was used with a simple point charge of –0.82e at the oxygen atom, and charges of 0.41e on each of the hydrogen atoms. The O-H bond length was 0.1 nm with a $109^{\circ}\ 28'$ angle for the H-O-H bond. Both the bond length and bond angle for water are constrained by the SHAKE method [21]. All ions were treated as single Lennard-Jones centers, with the parameters for energy (ϵ_{ij}) and distance (σ_{ij}) taken from published literature [22,16,17]. Periodic boundaries were applied, and the simulations carried out under constant pressure conditions. This method [23], allows the simulation box size to change so that the internal virial matches the external pressure.

The cell membrane was taken to comprise of Dioleoyl-phosphatidyl-choline (DPPC) lipid molecules. These are complex chain containing a large number of atoms, with a prominent "head" and two "tails" as shown in Fig. 6a. In order to ease the

computational burden and facilitate calculations in a reasonable amount of time, the complete DPPC molecule was reduced to a coarse grained model as shown in Fig. 6b. Thus, the choline, phosphate, glycerol, and methyl groups within DPPC were each aggregated to just one mega-molecule of large mass. The mega-molecules were treated as single Lennard-Jones centers, with the energy and distance parameters for each sub-group taken from the literature [16,17,22]. Such coarse-grained models have been used recently [24] to reduce the computational burden associated with an all-atom approach [25].

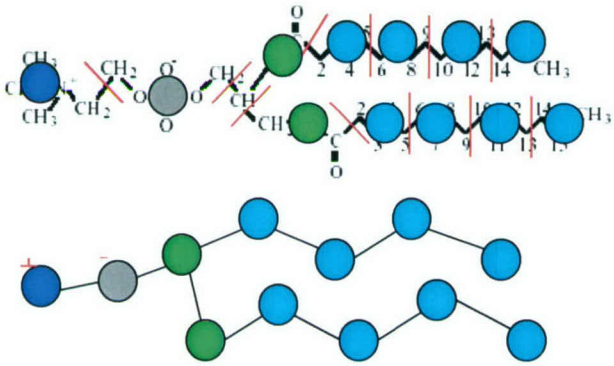

Fig.6. The dipalmitoyl -phosphatidyl-choline (DPPC) lipid molecule. (a) All atom representation, and (b) the coarse-grained model used.

For the actual simulation, a total of 128 DPPC chains (arranged on a uniform 8 x 8 square grid) and 3655 water molecules were used, yielding a ratio of 28.56:1 between water and the lipids. The total simulation volume was taken to a 6.8 nm x 6.8 nm x 6.8 nm cubic box. The lipid bilayer was taken to have an initial thickness of 4.5 nm. The starting configuration was created by assigning the DPPC molecules at each of the 64 locations within the square grid. The water molecules were randomly placed within the volume lying at the top and on the bottom of the DPPC layer. Due to our use of a constant pressure coupling, the initial size is not critical since the system continually adjusts to match the external pressure. In all cases, before starting the field-dependent calculations of interest, this system was allowed to reach its self-consistent energy minimized state by running the MD simulations at zero electric-field for 100 ps

Verification and validation of the MD code was first carried out, and the results compared with available reports. Towards this goal, simulations at zero electric field were first carried out in keeping with a recent publication by Lopez et al. [24]. Under this zero-field conditions, one does not expect pores to form, or for water molecules to pass through the membrane. Our results were in agreement with expectations and demonstrated this qualitative trend. This is clearly seen from the spatial electron density distribution result shown in Fig. 7. The absence of electron density over the central portion of the membrane is indicative of the inability of water molecules to pass through the DPPC membrane.

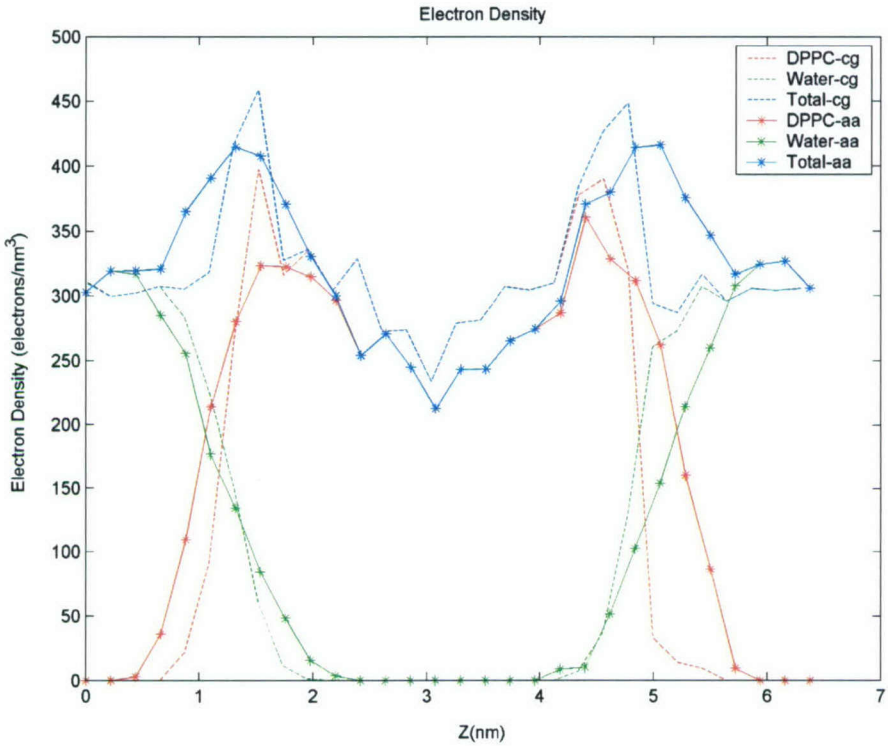

Figure 7. Molecular Dynamics simulation results showing the electron density distribution at zero electric field. Water molecules do not penetrate the central membrane region.

Next, the results of applying a realistic high-intensity, ultra-short electric pulse are presented and discussed. Snapshots showing the process of membrane configurational change are given in Fig. 8. Figure 8(a) shows the membrane to be well aligned (designated as the t = 0 ns instant) right after the energy minimization was performed. After about 4.8 ns, some structural rearrangement (i.e. defect formation) begins to form at the anode side (i.e., the membrane bottom) as shown in Fig. 8(b). A pore is then seen to form fairly quickly after the creation of the initial defect. In fact, a complete nano-pore formation is predicted within about 0.5 ns after the initial structural change. Obviously, most of the time for the electroporation process is taken up by the initial defect formation. A pore, formed at 5.3 ns, is shown in Fig. 8(c).

This result demonstrates several important points. First, there is a very good match between the MD result of Fig. 8, predictions of our distributed current model, and actual experimental data. In all cases, a nano-pore is predicted to occur within about 5-6 ns at these high field intensities applied to the cells. Since the pulse duration is typically longer than this time, ion transport (especially for ions with smaller radii) would be very likely. Second, the initial structural rearrangement and dipole re-orientation is a critical

step in the electroporation process. Once such an initial break-through is achieved, the poration process proceeds relatively quickly. Finally, the poration process has a polarity

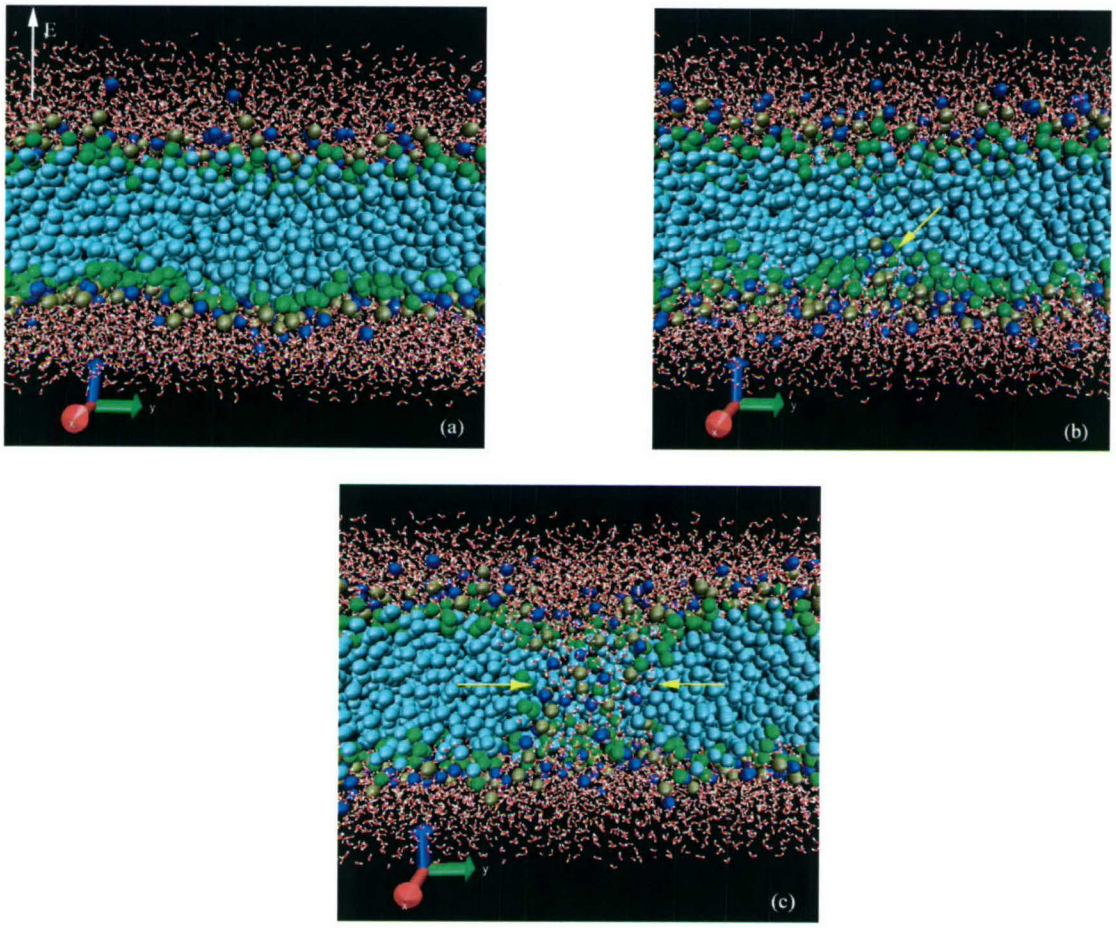

Fig. 8. MD snapshots of the electroporation process in a DPPC membrane. (a) Initial configuration at t = 0 ns; (b) Structural re-arrangement begins at the membrane bottom (anode side) at about t = 4.8 ns; (c) A pore predicted to form at t = 5.3 ns.

dependence, and begins on the anodic side of a membrane. The related physics can easily be understood by considering the dipolar configuration within the DPPC membrane. Fig. 9 shows a simple schematic of the membrane lipids with their dipoles located at the head-groups. For each DPPC chain, the head group contains a dipole with positive charge on Choline and the negative charge centered on the Phosphate group. Initially, with no electric field present, the dipoles are in random thermal motion with the positive charges residing on the outermost portions of the lipid. Electrical field induced defects are initiated by the movement of dipoles on the surface of the membrane. Defects start to form on the anode side of the membrane because positively charged molecules (e.g., Choline) on this side are forced to swing around (i.e., re-orient in the presence of a strong external electric field) and enter the membrane. However, this same applied electrical field, when acting on the dipoles located at the cathodic membrane surface merely works to stretch the dipoles without any molecular movement into the membrane

volume. Thus, Fig. 9(a) shows randomly distributed dipoles at the head groups on either side of the membrane as the initial configuration. Fig. 9(b) shows the alignment of

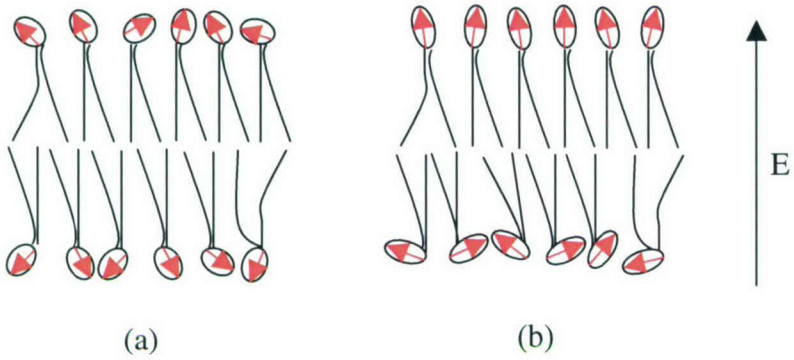

Fig. 9. Schematic of the pore initiation process at the DPPC membrane. The arrows present dipoles on the head groups of lipid molecules. (a) Initial configuration without an externally applied field, and (b) the configuration and expected movement of the dipole head groups upon the application of an external electric field.

dipolar head groups on the anodic side gradually deviating from the normal (equilibrium) orientation, and a defect starting to form.

If PS externalization is a pore-driven event, then this process should also start at the anode-side. Experimental observations do indicate just such an anode-side preference. The electrostatics provides an additional rationale for an anode-side event. Since the PS molecules residing on the inner leaflet are negatively charged, the externally applied electric field will tend to push out PS at the anode side, while pulling it inwards on the cathodic side. Coupling this with an anode-side pore formation event, leads to the collective effect of preferential PS externalization at the anode end. Fig. 10 is a simple

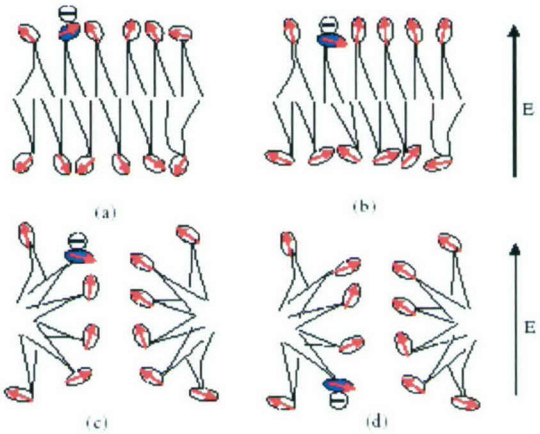

Fig. 10. Schematic of the pore initiation process within a DPPC-DPPS membrane. The arrows represent dipoles on the lipid head groups, and the shaded circle denotes the negative DPPS head group. (a) Initial configuration without an externally applied field; (b) configuration of the dipole head groups with an external field; (c) Nano-pore

formation with a DPPS molecule close to the pore; and (d) DPPS molecular movement to the outer leaflet of the membrane.

schematic demonstrating the dynamics. Initially (Fig. 10a), the dipoles at the DPPC lipids (shown as arrows) are randomly located, with a negative PS on the inner leaflet. With application of the electric field, the dipoles on the outer layer (anode-side) re-orient leading to defect initiation at the outer membrane surface. Eventually a pore forms (Fig. 10c), and the negatively charged PS begins to drift and diffuse towards the exterior surface. Results of MD simulations, shown in Figs. 11a-11d demonstrate the above more clearly. An initial snapshot of the membrane system is shown in Fig. 11(a), with the PS molecule located on one side of the membrane, opposite the anode. Fig. 11(b) shows a pore starting to form with some translocation of the PS chain at 3.2 ns. Due to a large electrostatic force on the PS head group (in the range of _10-10N), the chain is dragged half way to the anode side of the membrane along the wall of the nanopore at about _3.34 ns as shown in Fig. 11(c). Finally, in Fig. 11(d), the DPPS chain is on the other leaflet of the membrane at _3.61 ns. The MD simulation thus validates the pore-facilitated, field-assisted mechanism of PS externalization.

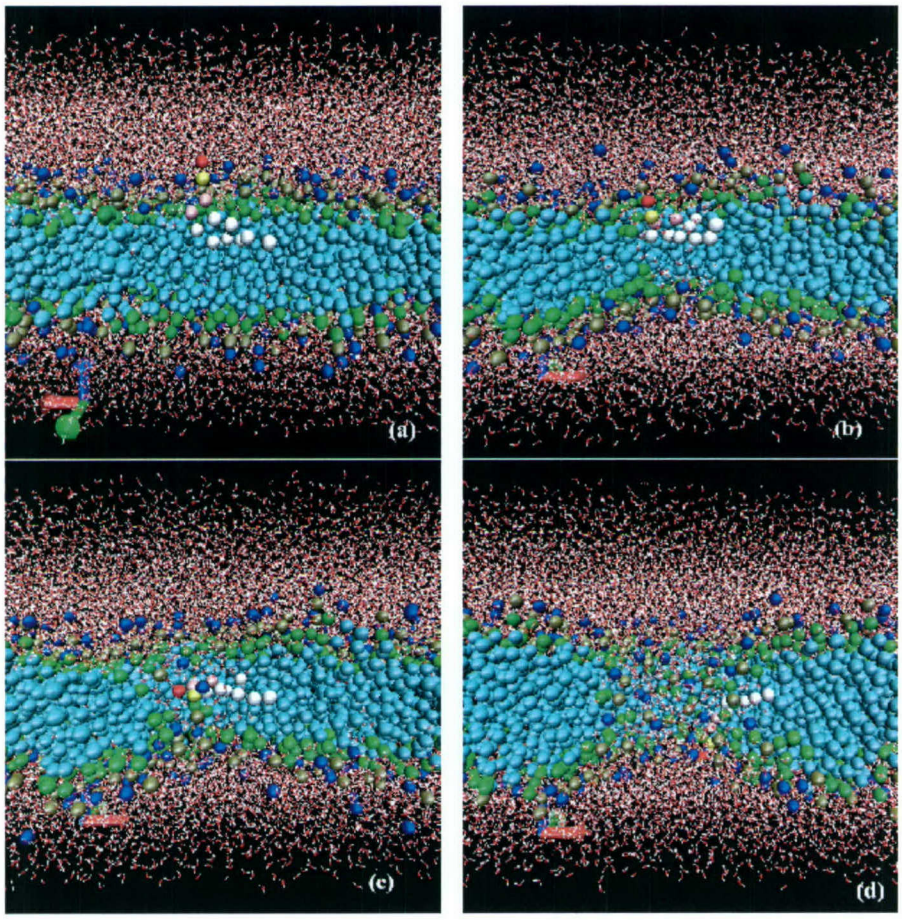

Fig. 11. Snapshots of the PS externalization process at a DPPC membrane. (a) Initial configuration at _ 0 ns; (b) A pore forms and DPPS starts to go along the pore wall at _

3.2 ns; (c) DPPS half way to externalization at _3.34ns; and (d) DPPS on the other leaflet of the membrane at _3.61 ns.

Objective II. Time Domain Dielectric Spectroscopy

The second objective of the Bio-Inspired Concepts grant focused on setting up and developing a state-of-the-art diagnostic system for monitoring the electrical properties of biological cells. It was based on utilizing Time Domain Dielectric Spectroscopy (TDDS) that allows for the measurement of frequency-dependent complex permittivity and conductance parameters of biological cells and tissues.

Accomplishments Under Objective II

Pulsed electric fields (PEFs) above a certain voltage threshold cause electroporation for microsecond pulses and intracellular effects for sub-microsecond pulses. Models describing these effects often depend on the electrical properties of the cell, which are altered by the PEF. We have used time domain dielectric spectroscopy (TDDS) to provide data for these models and to measure effects on cell suspension conductivity. In particular, single 50 μs and 10 ns pulses were applied to HL-60 cells, with the voltages chosen so the pulses have approximately the same energy. For 1.1 kV/cm, 50 μs pulses, the conductivity rose within a minute after the pulse and dropped dramatically approximately forty minutes after the pulse. For 78 kV/cm, 10 ns pulses, a brief delay prior to the conductivity rise was observed and the same drop in conductivity after approximately forty minutes was noted. For both pulse durations, higher voltages frequently led to membrane poration followed by a gradual recovery approximately thirty to forty minutes after the pulse. For 2 kV/cm, 50 μs pulses, significantly larger scatter in Trypan Blue uptake measurements were observed due to stronger effects on the cell membrane. By using a cell model, it was shown that a 50 μs pulse caused a much larger rise in membrane conductivity than a 10 ns pulse of the same energy.

Figure 12 shows a block diagram of the Time Domain Spectrometer (IDC Expertise, United Kingdom) based on a design by Feldman's group [26, 27]. An external pulse generator provides a 200 mV, 5 μs pulse with a 40-50 ps rise-time. The cell suspension can be placed in either a coaxial (high frequency) sample holder or a parallel plate (low frequency) sample holder [27]. The coaxial sample holder was chosen because it allowed for the use of fewer cells while still allowing measurements in the frequency range of interest. Due to the strong temperature dependence of the dielectric parameters, a thermostat (Julabo, US) was used to maintain sample cell at 25 C. After suitable signal processing [26, 27], a Fourier Transform was used to obtain the real and imaginary components of permittivity for the cell suspension. From this data, the permittivity and conductivity of the cell membrane, cytoplasm, nuclear envelope, and nucleoplasm could all be obtained for HL-60 using the two-shell model [26, 28].

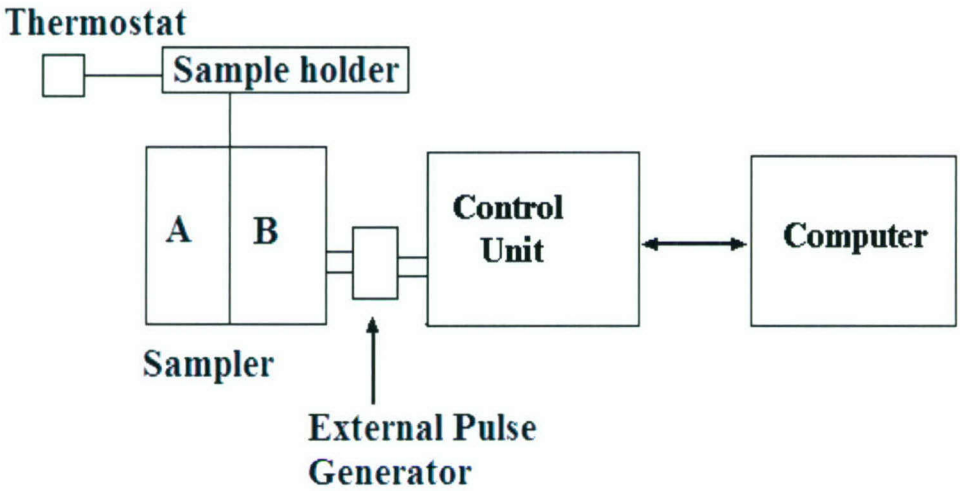

Figure 12. Block diagram of the TDDS system.

The results for the time-dependent permittivity (ϵ_m) obtained are shown in Fig. 13 after a typical 140 kV/cm, 10 ns pulse and after a typical 2 kV/cm, 50 μs pulse. For the 140 kV/cm pulse, ϵ_m rises from an initial control value of 5.70 to 8.02 within ninety seconds from the pulse, and then decreases to a 5.345 value fourteen minutes after the pulse. For the 2 kV/cm pulse, ϵ_m decreased from 3.04 to 2.35 thirty-five seconds after the pulse, and then rose to 3.32 about nineteen minutes after the pulse.

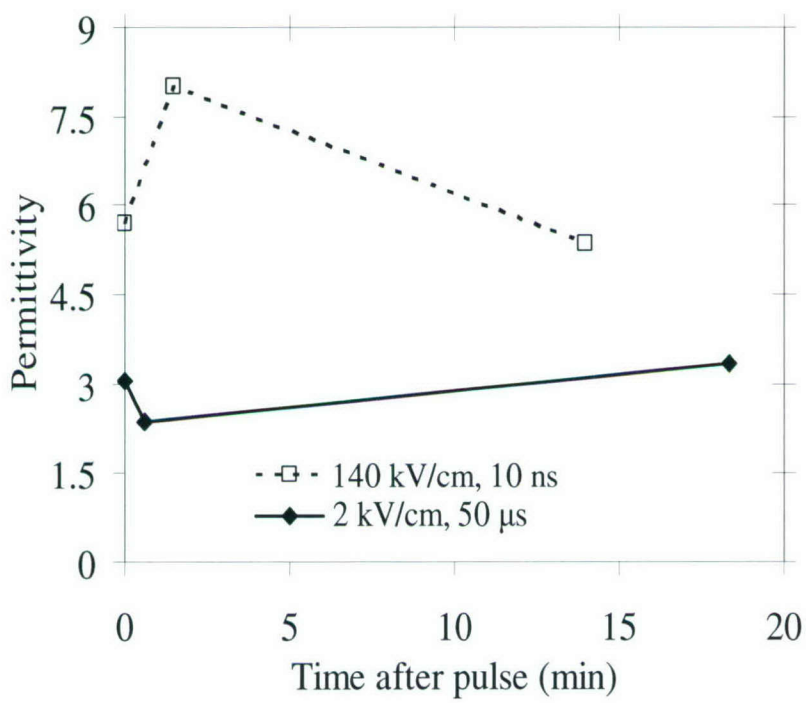

Fig. 13. Membrane permittivity (ϵ_m) of an HL-60 cell as a function of time after a 2 kV/cm, 50 μs pulse and a 140 kV/cm, 10 ns pulse.

Figure 14 shows the conductivity (σ_m) of an HL-60 cell membrane as a function of time after a 140 kV/cm, 10 ns pulse and after a 2 kV/cm, 50 μs pulse. For the 140 kV/cm pulse, σ_m rose from 7.5 x 10^{-6} S/m to 1.2 x 10^{-5} S/m about ninety seconds after the pulse. It then was seen to decrease to 6.7 x 10^{-6} S/m about fourteen minutes after the pulse. For 2 kV/cm pulse, σ_m rose from 3.6 x 10^{-6} S/m to 1.08 x 10^{-5} S/m thirty-five seconds after the pulse and 9 x 10^{-6} S/m about nineteen minutes after the pulse.

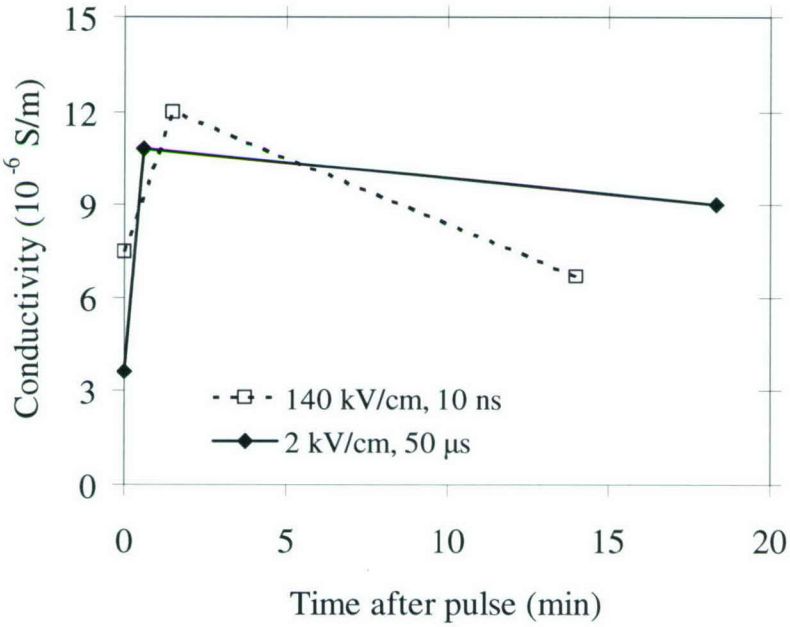

Fig. 14. Membrane conductivity (σ_m) of an HL-60 cell membrane as a function of time after a 140 kV/cm, 10 ns pulse and a 2 kV/cm, 50 μs pulse.

The next step in this analysis is to utilize the full two-shell model to determine the electrical properties of each component of the cell [28]. A complete and rigorous analysis has so far been difficult for a variety of reasons. One problem is that the two-shell model is very sensitive to the geometric parameters of the cell [28], which can be greatly altered by the PEF. Moreover, electroporation and intracellular manipulation are inherently anisotropic.

Objective III. Cellular Measurements of High-Field Pulse Effects

A final portion of the Bio-Inspired Concepts grant focused on experimental measurements of cell response to pulsed electric fields.

Accomplishments Under Objective III

The effects of nanosecond (10-300ns) pulsed electric fields (nsPEF) on mammalian cell structure and function were probed. As the pulse durations decreased,

effects on the plasma membrane (PM) correspondingly decreased and effects on intracellular signal transduction mechanisms increased. When nsPEF-induced PM electroporation effects did occur, they were distinct from classical PM electroporation effects, suggesting unique, nsPEF-induced PM modulations. NsPEF with durations and electric field intensities were seen to induce apoptosis in mammalian cells with a well-characterized phenotype typified by externalization of phosphatidylserine on the outer PM and activation of caspase proteases.

Some of the relevant experimental details are summarized below.

Cell culture: HL-60 and Jurkat cells were obtained from and cultured as recommended by American Type Culture Collection as described in detail elsewhere [13, 29, 30]. Cells were removed from log phase growth and suspended in Hanks Balanced Salt Solution (HBSS) or Tyrodes buffer.

Administration of nsPEF: Cell suspensions (7.7 x 106 cells/ml; 106 cells/130μl) were loaded into the BioRad gene Pulser® cuvettes (Bio-Rad laboratories; Hercules, CA) prior to nsPEF pulsing. The pulse was delivered to the load, via either a 0.1, 0.2, or 0.4 cm cuvette containing cell suspension, by means of a cable pulse generator. Briefly, the generator consists of a pulse-forming network (PFN), - five 50 cables in parallel and a spark gap in atmospheric air as a nanosecond closing switch. Post pulse the cell suspension was removed from the pulsing cuvette and assayed.

Determination of plasma membrane integrity: HL-60 or Jurkat cells were exposed to nsPEF in the presence of ethidium homodimer-1 or propidium iodide (Molecular Probes, Eugene, OR) and analyzed by flow cytometry. Values are expressed as the geometric mean fluorescence intensity and/or as the percentage of cells that exhibited fluorescence.

Effect of nsPEF on apoptosis induction: Apoptosis was determined using flow cytometry and well defined apoptosis characteristics including maintenance of membrane integrity as determined by the exclusion of ethidium homodimer, the presence of annexin-V binding as a marker for phosphatidylserine externalization on the plasma membrane of intact cells, and the presence of caspase activation using two different assays.

Flow cytometry: Flow cytometry was carried out as previously described. Briefly, ~10^6 cells were exposed to nsPEF in electroporation cuvettes. Cell suspensions (1.5 x 10^4 /ml) were then analyzed using a Becton-Dickinson FACS calibur flow cytometer. Fluorescence emission was collected with interference bandpass filter sets for (FL1-H) and (FL2-H). Data was stored and analyzed by CellQuest software.

Based on an electric model of biological cells, it was predicted that as the pulse duration decreases effects on the plasma membrane would decrease. To test this hypothesis directly, Jurkat or HL-60 cells were exposed to pulsed fields with durations of 10 or 60 ns and the number and amplitude of the pulses were varied as shown in figure 15. The cells were treated with the pulses in the presence of ethidium homodimer, a fluorescent, membrane impermeable DNA stain that is used as a marker for plasma

membrane integrity, and then evaluated for fluorescence by flow cytometry. Panels A and B show results from Jurkat cells that were exposed to single pulses of 10 and 60 ns, respectively, with increasing electric fields. The level of fluorescence is a direct indicator of levels of effects on plasma membrane electroporation. For any given electric field, effects on plasma membrane integrity were less for the shorter pulses. The thresholds for breaching plasma membrane integrity were between 150 and 300 kV cm^{-1} for 10 ns pulses and between 26 and 40 kV cm^{-1} for 60 ns pulses. Thus, higher electric fields were required to affect the plasma membrane for 10 ns versus 60 ns pulses. Similar effects were observed for HL-60 cells (data not shown). Panels C and D show results from HL-60 cells for 10 and 60 ns pulses with the electric field adjusted to provide a similar energy density with increasing pulse numbers. Effects on the plasma membrane increased with increasing pulse number for both 10 and 60 ns pulses, but effects at 10 ns were less than the effects at 60 ns for any given pulse number.

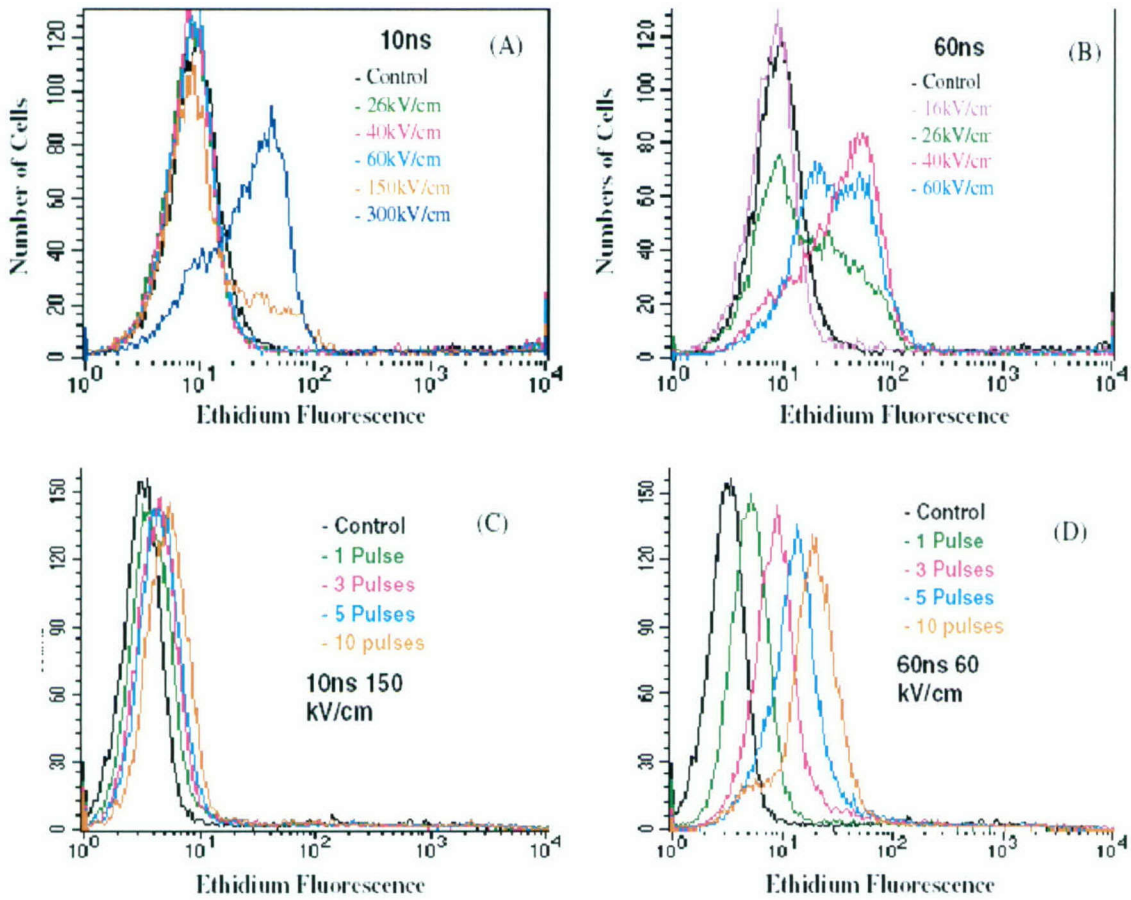

Figure 15. Data showing that as the pulse number, durations and/or the electric field intensities decrease, effects on the plasma membrane (PM) also decrease.

In order to compare the effects of nsPEF and classical electroporation on plasma membrane integrity, Jurkat cells were exposed to a single 10 ns pulses at 150 kV cm^{-1} shown in figure 16 (panel A) or, a single 6 ms pulse at 0.5 kV cm^{-1} in the presence of ethidium homodimer and analyzed by flow cytometry. The effects of the 10 ns pulse on plasma membrane integrity were minimal. In contrast, the classical electroporation pulses, which provided an energy density 50% lower than the 10 ns pulse, resulted in considerable increases in ethidium homodimer fluorescence, indicating significant disruption of the plasma membrane. When ethidium homodimer was added 10 or 45 min after exposure to each of the pulsed electric fields, no increase in fluoresce was observed after the 10 ns pulse, but significant fluorescence was observed after the classical electroporation pulses (data not shown). These results indicate that nsPEF have minimal effects on the plasma membrane that are short lived, while classical plasma membrane electroporation pulses have considerable longer lasting effects on the plasma membrane and are thus functionally different.

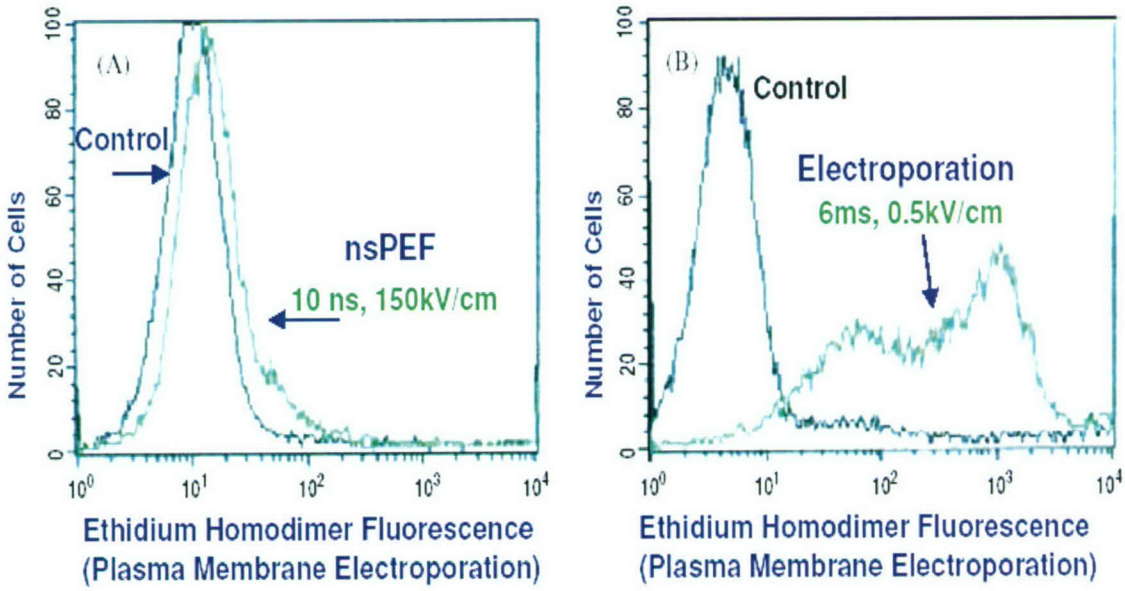

Figure 16. Classical plasma membrane electroporation and nsPEF conditions have significantly different effects on plasma membrane integrity.

As illustrated in figure 17, HL-60 cells were exposed to nsPEF with durations of 10 ns (top panels) or 60 ns (bottom panels) and increasing electric fields as indicated. Cells were exposed to nsPEF in the presence of ethidium homodimer as a marker for plasma membrane integrity (left panels) during the pulses and then Annexin-V-FITC was added as an apoptosis marker for PS externalization (right panels). Cells were analyzed for fluorescence by flow cytometry 10 min post-pulse. As indicated by ethidium homodimer fluorescence (left panels) none of the conditions led to significant losses in plasma membrane integrity. In these experiments, no significant losses of plasma membrane integrity occurred; only 3% of the cells exhibited minimal ethidium fluorescence at 60 ns and 60 kV cm^{-1}. In contrast, Annexin-V-FITC binding was

observed at 10 ns with electric fields of greater than 150 kV cm^{-1} , and at 60 ns with electric fields of greater than 26 kV cm^{-1}. Like nsPEF-induced effects on plasma membrane integrity, lesser effects were observed for PS externalization at shorter pulse durations, and higher electric fields were required to induce PS externalization as the pulse duration decreased. Thus, it was possible to observe nsPEF-induced PS externalization under conditions that did not include loss of plasma membrane integrity.

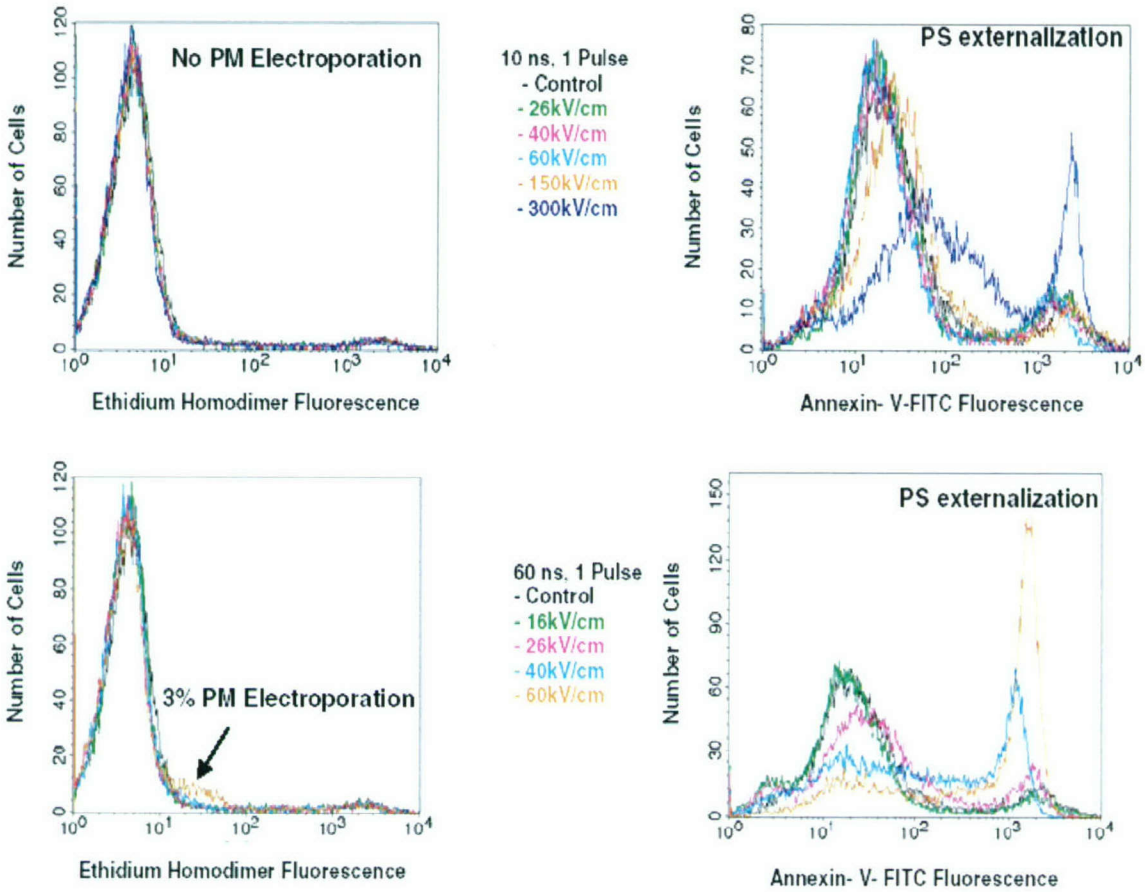

Figure 17. Phosphatidylserine (PS) externalization occurs independent of loss of plasma membrane integrity in response to nsPEF.

SUMMARY

A comprehensive modeling and experimental effort was carried out to develop an understanding of cellular bio-response to short duration, high-intensity electric fields. The simulation capability included macroscopic models for determining the time-dependent spatially-variable electric potential and current flows at single cells. This provides the

means of predicting changes in the transmembrane voltages at the plasma and other intra-cellular membranes. This voltage change is thought to be the primary driver in bringing about change (both reversible and irreversible) in bio-systems. The macroscopic model also provides for predictions of heating and internal temperature rises.

The macroscopic model was then coupled to a microscopic, nano-simulator to probe the sub-cellular response at the molecular level. Many of the observed details such as PS externalization, the time scales for pore formation, and their probable diameters were predicted. The results agreed well with the experimental data, and provide a logical basis for the lack of Propidium Iodide transport during cell exposure to pulsed voltages.

For accurate predictions, the relevant parameters of the bio-system need to be known or to be obtained. This was done within our group by developing the Time Domain Dielectric Spectroscopy method. The system is operational, and yields data on the conductivity and permittivities of cells and its organelles. This is a useful and important development.

Finally, cellular response were measured based on a variety of techniques, including flow cytometry, optical microscopy and imaging. The central results were: (i) There is a critical electric field (or transmembrane potential) below which no cell death is observed. Above the critical field, there was a rapid transition from 100% to 0% cell survival. (ii) The critical membrane voltage for irreversible electroporation decreases with increasing pulse width and multiple pulses with an asymptotic value of ~ 1 volt for long pulse lengths. (iii) Transmembrane voltage for irreversible electroporation scaled with constant pulse energy for pulse lengths less than 5 μs. (iv) PS externalization leading to cell death through macrophage action can be electrically triggered. Pore formation can be reversible at the short nano-second pulse durations.

This study would be indicative of the following conclusions: (i) It may be energy efficient to use short pulses for cell death. The elimination of heat dissipation in the medium would contribute to this efficiency. (ii) Selective targeting of cells for apoptosis appears to be possible through the use of ultra-short pulses. (iii) The ability to extract energy with directed motion and transport from low-amplitude fluctuations appears to be possible in cell membranes based on spatially non-uniform potentials.

REFERENCES

1. R. P. Joshi, Q. Hu and K. H. Schoenbach, "Modeling Studies of Cell Response to Ultrashort, High-Intensity Electric Fields – Implications for Intracellular Manipulation", IEEE Trans. Plasma Science **32**, 1677 (2004).

2. S. J. Beebe, P. F. Blackmore, J. White, R. P. Joshi, and K. H. Schoenbach, "Nanosecond Pulsed Electric Fields Modulate Cell Function Through Intracellular Signal Transduction Mechanisms", Physiological Measurement **25**, 1077 (2004).

3. K. H. Schoenbach, R. P. Joshi, J. Kolb, N. Chen, M. Stacey, P. Blackmore, E. S. Buescher, and S. J. Beebe, "Ultrashort Electrical Pulses Open A New Gateway Into Biological Cells", Proc. IEEE **92**, 1122 (2004).

4. N. Chen, K. H Schoenbach, J. F. Kolb, R. J. Swanson, A. L. Garner, J. Yang, R. P. Joshi, and S. J. Beebe, "Leukemia Cell Intracellular Responses to Nanosecond Electric Fields," Biochemical and Biophysical Research Communications **317**, 421 (2004).

5. R. P. Joshi, Q. Hu, K. H. Schoenbach, and S. J. Beebe, "An Energy-Landscape Model Analysis for Irreversibility and It's Pulse Width Dependence in Cells Subjected to a High-Intensity, Ultrashort Electric Pulse", Phys. Rev. E **69**, 051901 (2004).

6. R. P. Joshi, Q. Hu, and K. H. Schoenbach, "Dynamical Modeling of Cellular Response to Short-Duration, High-Intensity Electric Fields", IEEE Trans. Dielectr. Electr. Insul. **10**, 778 (2003).

7. I. Ermolina, Y. Polevaya, Y. Feldman, B. Ginzburg and M. Schlesinger, "Study of Normal and Malignant White Blood Cells by Time Domain Dielectric Spectroscopy," IEEE trans. On Dielectrics and Electrical Insulation **8**, 253 (2001).

8. M. Smoluchowski, "Drei vortrage uber diffusion, Brownsche bewegung und koagulation von kolloidteilchen," Physik Zeits. **17**, 557 (1916).

9. S. Chandrasekhar, "Stochastic Problems in Physics and Astronomy," Rev. Mod. Phys. **15**, 1 (1943).

10. R. P. Joshi and K. H. Schoenbach, "Electroporation Dynamics in Biological Cells Subjected to Ultrafast Electrical Pulses : A Numerical Simulation Study," Phys. Rev. E. **62**, 1025 (2000).

11. S. A. Freeman, M. A. Wang, and J. C. Weaver, "Theory of Electroporation of Planar Bilayer Membranes: Predictions of the Aqueous Area, Change in Capacitance, and Pore-Pore Separation," Biophys. J., **67**, 42 (1994).

12. V. F. Pastushenko, Yu A. Chhizmadzhev, "Electrical Breakdown of Lipid Vesicles," Biofizika **28**, 1036 (1983).

13. S. J. Beebe, P. M. Fox, L. J. Rec, L. K. Willis, and K. H. Schoenbach, "Nanosecond, High-Intensity Pulsed Electric Fields Induce Apoptosis in Human Cells," FASEB Journal **17**, 1493 (2003).

14. N. Agmon and J. J. Hopfield, "CO Binding to Heme Proteins: A Model for Barrier Height Distributions and Slow Conformational Changes," J. Chem. Phys. **79**, 2042 (1983).

15. P. G. Wolynes, J. N. Onuchic, and, D. Thirumalai, "Navigating the Folding Routes," Science **267**, 1619 (1995).

16. D. van der Spoel, A. R. van Buuren, E. Apol, P. J. Meulenhoff, D. P. Tieleman, A. L. Sijbers, R. van Drunen, and H. J. C. Berendsen, *Gromacs User Manual Version 1.2*, 1996.

17. H. J. C. Berendsen, D. van der Spoel, and R. van Drumen, "GROMACS: A Message-Passing Parallel Molecular Dynamics Implementation," Comp. Phys. Comm. **91**, 43 (1995).

18. H. J. C. Berendsen, J. P. Postma, W. F. Gunsteren, and J. Hermans, in *Intermolecular Forces*; Edited by B. Pullman (Reidel: Dordrecht, The Netherlands, 1981), pp 331-342.

19. D. P. Tieleman, S. J. Marrink, and H. J. C. Berendsen, Biochimica et Biophysica Acta **1331**, 235 (1997).

20. M. P. Allen and D. J. Tildesley, *Computer Simulations of Liquids* (Clarendon Press, Oxford, 1987).

21. W. F. van Gunsteren and H. J. C. Berendsen, "Algorithms for Macromolecular Dynamics and Constraint Dynamics," Mol. Phys. **34**, 1311 (1977).

22. E. Egberts and H. J. C. Berendsen, "Molecular Dynamics Simulation of a Smectic Liquid Crystal with Atomic Detail," J. Chem. Phys. **89**, 3718 (1988).

23. H. J. C. Berendsen, J. P. M. Straatsma, W. F. van Gunsteren, A. DiNola, and J. R. Haak, "Molecular Dynamics with Coupling to an External Bath," J. Chem. Phys. **81**, 3684 (1984).

24. C. F. Lopez, P. B. Moore, J. C. Shelley, M. Y. Shelley, and M. L. Klein, "Computer Simulation Studies of Biomembranes Using a Coarse Grain Model," Comp. Phys. Comm. **147**, 1 (2002).

25. D. P. Tieleman, H. Leontiadou, A. E. Mark, and S. J. Marrink, "Simulation of Pore Formation in Lipid Bilayers by Mechanical Stress and Electric Fields," Comp. Phys. Comm. **125**, 6382 (2003).

26. Yu. Feldman, I. Ermolina, and Y. Hayashi, "Time domain dielectric spectroscopy study of biological systems," IEEE Trans. Diel. Elec. Insul. **10**, 728 (2003).

27. Y. Feldman, A. Andrianov, E. Polygalov, I. Ermolina, G. Romanychev, Y. Zuev, B. Milgotin, "Time domain dielectric spectroscopy: An advanced measuring system," Review of Scientific Instruments **67**, 3208 (1996).

28. Y. Polevaya, I. Ermolina, M. Schlesinger, B-Z. Ginzburg, and Y. Feldman, "Time domain dielectric spectroscopy study of human cells II. Normal and malignant white blood cells," Biochimica et Biophysica Acta **1419**, 257 (1999).

29. S. J. Beebe, P. M. Fox, L. J. Rec, K. Somers, R. H. Stark, and K. H. Schoenbach, "Nanosecond Pulsed Electric Field (nsPEF) Effects on Cells and Tissues: Apoptosis Induction and Tumor Growth Inhibition," IEEE Trans. Plasma Sci. **30,** 286 (2002).

30. S. J. Beebe, J. White, P. F. Blackmore, Y. Deng, K. Somers, and K. H. Schoenbach, "Diverse Effects of Nanosecond Pulsed Electric Fields on Cells and Tissues," DNA Cell Biol. **12,** 785 (2003).

PERSONNEL

(A) Old Dominion University:

ECE Faculty
Dr. Ravindra Joshi (PI), Professor
Dr. Karl H. Schoenbach (Co-PI), Eminent Professor

ECE Research Faculty
Dr. Juergen Kolb (Part-time)

Graduate Students
Qin Hu – Ph.D. student (Graduated in 2004)
Allen Garner – M.S. student (Graduated in 2004)
S. Viswanadham – M.S. student (Graduated in 2003 - 2004)
S. Viswanadham – Ph.D. student (2004 - Present)

(B) Eastern Virginia Medical School:

Faculty
Dr. Stephen J. Beebe (Co-PI), Associate Professor

PUBLICATIONS

Research publications resulting from the work performed are provided in this report. This published material was based on research sponsored by the Air Force Research Laboratory, under the agreement number **F49620-01-1-0506.** The U.S. Government is

authorized to reproduce and distribute reprints for Governmental purposes notwithstanding any copyright notation thereon.

Journal Papers

1. Q. Hu, R. P. Joshi, and K. H. Schoenbach, "Simulations of Nanopore Formation and Phosphatidylserine Externalization in Lipid Membranes Subjected to a High-Intensity, Ultra-Short Electric Pulse," submitted for publication, February 2005.

2. Q. Hu, S. Viswanadham, R. P. Joshi, K. H. Schoenbach, S. J. Beebe and P. F. Blackmore, "Simulations of Transient Membrane Behavior in Cells Subjected to a High-Intensity, Ultra-Short Electric Pulse," Phys. Rev. E **71**, 031914 (2005).

3. A. L. Garner, N. Chen, J. Yang, J. Kolb, R. J. Swanson, S. J. Beebe, R. P. Joshi, and K. H. Schoenbach, "Time Domain Dielectric Spectroscopy Measurements of HL-60 Cells Suspensions after Microsecond and Nanosecond Electrical Pulses", IEEE Trans. Plasma Science **32**, 2073 (2004).

4. R. P. Joshi, Q. Hu and K. H. Schoenbach, "Modeling Studies of Cell Response to Ultrashort, High-Intensity Electric Fields – Implications for Intracellular Manipulation", IEEE Trans. Plasma Science **32**, 1677 (2004).

5. S. J. Beebe, P. F. Blackmore, J. White, R. P. Joshi, and K. H. Schoenbach, "Nanosecond Pulsed Electric Fields Modulate Cell Function Through Intracellular Signal Transduction Mechanisms", Physiological Measurement **25**, 1077 (2004).

6. K. H. Schoenbach, R. P. Joshi, J. Kolb, N. Chen, M. Stacey, P. Blackmore, E. S. Buescher, and S. J. Beebe, "Ultrashort Electrical Pulses Open A New Gateway Into Biological Cells", Proc. IEEE **92**, 1122 (2004).

7. N. Chen, K. H Schoenbach, J. F. Kolb, R. J. Swanson, A. L. Garner, J. Yang, R. P. Joshi, and S. J. Beebe, "Leukemia Cell Intracellular Responses to Nanosecond Electric Fields," Biochemical and Biophysical Research Communications **317**, 421 (2004).

8. R. P. Joshi, Q. Hu, K. Schoenbach, and S. Beebe, "An Energy-Landscape Model Analysis for Irreversibility and It's Pulse Width Dependence in Cells Subjected to a High-Intensity, Ultrashort Electric Pulse", Phys. Rev. E **69**, 051901 (2004).

9. R. P. Joshi, Q. Hu, and K. H. Schoenbach, "Dynamical Modeling of Cellular Response to Short-Duration, High-Intensity Electric Fields", IEEE Trans. Dielectr. Electr. Insul. **10**, 778 (2003).

10. R. P. Joshi, Q. Hu, K. H. Schoenbach, and S. J. Beebe, "Simulations of Electroporation Dynamics and Shape Deformations in Biological Cells Subjected to High Voltage Pulses", IEEE Trans. Plasma Sci. **30**, 1536 (2002).

11. R. P. Joshi and K. H. Schoenbach, "A Mechanism for Membrane Electroporation Irreversibility Under High-Intensity, Ultrashort Electrical Pulse Conditions", Physical Review E **66**, 052901 (2002).

12. R. P. Joshi, Q. Hu, K. H. Schoenbach, and H. P. Hjalmarson, "Improved Energy Model for Membrane Electroporation in Biological Cells Subjected to Electrical Pulses", Phys. Rev. E **65**, 041920 (2002).

Journal Articles (Submitted)

1. Q. Hu, R. P. Joshi, and K. H. Schoenbach, "Simulations of Nanopore Formation and Phosphatidylserine Externalization in Lipid Membranes Subjected to a High-Intensity, Ultra-Short Electric Pulse," submitted for publication, February 2005.

Conference Presentations

1. R. P. Joshi, Q. Hu, V. K. Lakdawala, and K. H. Schoenbach, "Modeling the Dynamical Response of Biological Cells," IEEE Int'l Conf. On Dielectrics and Electrical Insulation, Denver, CO, Oct. 17-20, 2004.

2. G. Chen, N. Chen, A. L. Garner, J. Kolb, R. J. Swanson, S. Beebe, R. P. Joshi and K. H. Schoenbach, "Conductivity Changes in Jurkat Cell Suspensions Subjected to Ultrashort Electric Pulses", 3rd International Workshop on Biological Effects of Electro-Magnetic Fields, 4 Oct. – 8 Oct. 2004, Kos, Greece.

3. K. H. Schoenbach, R. P. Joshi, J. Kolb, S. Buescher, and S. J. Beebe, "Subcellular Effects of Nanosecond Electrical Pulses", 26th IEEE Int'l. Conf. On Engineering in Medicine and Biology, 1 Sept. – 5 Sept. 2004, San Francisco, USA.

4. A. L. Garner, J. Yang, N. Chen, J. Kolb, K. C. Loftin, R. J. Swanson, S. Beebe, R. P. Joshi, and K. H. Schoenbach, "Altering Dielectric Properties of Human Cancer Cells by Varying Electrical Pulse Durations", Int'l Conf. On Plasma Science (ICOPS), 28 June – 1 July, 2004, Baltimore, USA.

5. A. L. Garner, J. Yang, N. Chen, J. Kolb, K. C. Loftin, R. J. Swanson, S. Beebe, R. P. Joshi, K. H. Schoenbach, "Electrical Pulse-Induced Changes In Hl-60 Dielectric Properties", Bio-Electromagnetic Society Conference, 21 June – 24 June, Washington DC, USA.

6. S. Xiao, J. F. Kolb, C. Bickes, Y. Minamitani, M. Laroussi, R. P. Joshi, and K. H. Schoenbach, "Recovery Of High Power Water Switches", Power Modulators Conf., 23 May – 26 May, San Francisco, 2004.

7. K. H. Schoenbach, R. P. Joshi, J. F. Kolb, N. Chen, M. Stacey, P. Blackmore, E. S. Buescher, And S. J. Beebe, "Ultrashort Electrical Pulses Open A New Gateway Into Biological Cells", Power Modulators Conf., 23 May – 26 May, San Francisco, 2004.

8. R. P. Joshi, Q. Hu, K. H. Schoenbach, and V. K. Lakdawala, "Modeling the Dynamical Response Of Biological Cells Stressed by Nanosecond, High-Intensity Electric Fields", IEEE Int'l Conf. On Dielectrics and Electrical Insulation, Boulder, CO, Oct. 17-20, 2004.

9. R. P. Joshi, Q. Hu, and K. H. Schoenbach, "Modeling Studies Of Cell Response To Ultrashort, High-Intensity Electric Fields For Intracellular Manipulation," Workshop on Bio-Dielectrics at the IEEE Int'l Conf. On Dielectrics and Electrical Insulation, Albuquerque, NM, Oct. 19-22, 2003 (***invited***).

10. A L. Garner, J. Yang, N. Chen, J. Kolb, K. C. Loftin, R. J. Swanson, S. Beebe, R. P. Joshi, and Karl H. Schoenbach, "Effects of Electrical Pulses on the Dielectric Properties of Biological Cells," IEEE Int'l Conf. On Dielectrics and Electrical Insulation, Albuquerque, NM, Oct. 19-22, 2003

11. A.L. Garner, N. Chen, J. F. Kolb, K. C. Loftin, R. J. Swanson, S. J. Beebe, R. P. Joshi, and K. H. Schoenbach, "Effects of Electrical Pulses on the Dielectric Properties of Biological Cells," ElectroMed Conference, San Antonio, TX, June 11-13, 2003.

12. R. P. Joshi, Q. Hu, And K. H. Schoenbach, "Modeling Studies Of Cell Response To Ultrashort, High-Intensity Electric Fields–Implications For Intracellular Manipulation And Ion Transport," ElectroMed Conference, San Antonio, TX, June 11-13, 2003.

13. K. H. Schoenbach, R. P. Joshi, S. J. Beebe, and E. S. Buescher, "Nanosecond Electrical Pulses Open a Gateway into Biological Cells," Int'l. Meeting of the German Physical Society, Aachen, Germany, Mar. 2003.

14. R. P. Joshi, "Dynamical Modeling of Cellular Response to Short High-Intensity Electric Fields," IEEE Conf. On Dielectrics and Electrical Insulation (Bio-Electrics Workshop), Cancun, Mexico, Oct. 2002 (***invited*).**

INTERACTIONS RELATED TO PROJECT

1. Interactions with scientists at the AFOSR Research Laboratory, Brooks Air Force Base (M. Murphy, W. Rogers, A. Pakhomov, and C. Beason). This led to modeling studies of electro-stimulation by a nanosecond voltage pulse. The results were accepted for publication, and appeared is as a journal article in the Special Issue of the IEEE

Transactions on Plasma Science (August 2004 issue, Vol. **32**, pp. 1687-1695). The contribution was titled: "Modeling Electrode-Based Stimulation of Muscle and Nerve by Ultra-Short Electric Pulses".

2. Guest editor, together with W. R. Rogers and A. Pakhomov, on a special issue on: "Non-thermal Medical and Biological Applications of Ionized Gases and Electromagnetic Fields" for the IEEE Transactions on Plasma Science

RECOGNITION

1. Professor Ravindra P. Joshi : Old Dominion University, Rufus Tonelson Annual Award for Faculty Excellence in Research and Teaching – 2004.

2. Professor Ravindra P. Joshi : Certificate of Appreciation, Air Force Research Laboratory, San Antonio, TX (2003).

3. Professor Karl H. Schoenbach : Research Excellence Award, Dept. of Electrical & Comp. Engineering, ODU (2003).

4. Professor Ravindra P. Joshi : 18th Annual Research Award, Old Dominion University (2002).

5. Professor Ravindra P. Joshi : Research Excellence Award, Dept. of Electrical & Comp. Engineering, ODU (2002).

NEW DISCOVERIES, INVENTIONS & PATENTS

None.